5-9-2015

Control of Spiking Activity by Persistent Sodium and Hyperpolarization-activated Currents

Hasti Ghabel
Biology Department

CONTROL OF SPIKING ACTIVITY BY PERSISTENT SODIUM AND HYPERPOLARIZATION-ACTIVATED CURRENTS

by

HASTI GHABEL

Under the Direction of Gennady Cymbalyuk, PhD

ABSTRACT

The properties of spiking activity such as the spike shape are crucial for normal and homeostatic functioning of a neuron. For example, the spike width determines the calcium influx and correspondingly the intracellular calcium concentration ($[Ca^{2+}]_i$), which plays key roles in variety of cellular processes from basic neurotransmitter release to gene transcription. Dantrolene, a specific inhibitor of ryanodine channel-mediated calcium release from intracellular calcium stores, inhibits two main ionic currents in B5 neurons of mollusk *Helisoma trivolvis*, persistent sodium current and hyperpolarization-activated current (h-current). We developed a model of the neuronal activity of B5 neuron and investigated how the parameters of persistent sodium current (I_{NaP}) and h-current (I_H) affect the spike shape. In the model of B5 neuron, either

removal of I_H by shifting its voltage of half-activation to more hyperpolarized values or removal of I_{NaP} by reducing its maximal conductance decreases the spike width and shifts the minimum after-hyperpolarization potential (mAHP) towards more negative values. We showed in the model that the spike width linearly correlated with calcium influx into the cell. In this model, the spike width is controlled by the inactivation variables of fast sodium, persistent sodium, and calcium currents at the spike threshold. The activation of the h-current governs membrane potential during the inter-spike interval (ISI) and determines the values of these inactivation variables. At mAHP of spike, the activation of the h-current was the only variable that substantially affected the spike width and mAHP. In conclusion, removal of the h-current or the persistent sodium current reproduced the dantrolene effects on spike shape and reduced the calcium influx through membrane calcium channels. The inactivation variables of inward currents, modulated by activation of the h-current, describe the mechanism governing the spike width.

INDEX WORDS: action potential, spike width, minimum after-hyperpolarization potential (mAHP), inactivation variable, hyperpolarization-activated current, persistent sodium current, intracellular calcium concentration ($[Ca^{2+}]_i$).

CONTROL OF SPIKING ACTIVITY BY PERSISTENT SODIUM AND HYPERPOLARIZATION-ACTIVATED CURRENTS

by

HASTI GHABEL

A Thesis Submitted in Partial Fulfillment of the Requirements for the Degree of

Master of Science

in the College of Arts and Sciences

Georgia State University

2015

CONTROL OF SPIKING ACTIVITY BY PERSISTENT SODIUM AND HYPERPOLARIZATION-ACTIVATED CURRENTS

by

HASTI GHABEL

Committee Chair: Gennady Cymbalyuk

Committee: Vincent Rehder

William Walthall

Electronic Version Approved:

Office of Graduate Studies

College of Arts and Sciences

Georgia State University

May 2015

DEDICATION

I dedicate this work to my beloved husband Vahid, who always encouraged me and supported me during the journey of my Master program. He, with his nice smile and support, helped me to pass through every difficulty during this project. Also, I would like to deeply thank my lovely parents for being always supportive beside me throughout my life to become a successful and happy person in the society.

ACKNOWLEDGEMENTS

I would like to deeply thank my adviser, Dr. Gennady Cymbalyuk. I really appreciate his help as he accepted me to join his lab from the beginning of my program. He helped me to grow in the research field and become stronger as a scientist. I believe that his guidance and unconditional support helped me to go through the difficulties and to have the confidence to pursue my future educational and professional goals.

I would also like to thank my committee, Dr. Vincent Rehder and Dr. William Walthall. I had the opportunity to learn from Dr. Rehder and take his guidance not only about my Master project but also about making important decisions for my future goals. Dr. Walthall advised me with my coursework not only as my committee but also as the director of Biology department.

Further, I am so grateful to have Will Barnett as one of my lab colleagues. He enthusiastically shared his scientific skills and knowledge in neuroscience and computer programing. Also, I appreciate the friendship and help from my other lab members, Jingjing Fu Cannon and Jessica Green. I'd also like to thank Kyle Harris as he helped me in the very beginning of this project.

In addition, the journey of collaborating with Dr. Rehder's lab gave me the opportunity to work with Dr. Liana Artinian and learn from her knowledge and her enthusiasm for novel discoveries. Additionally, I'd like to thank Stephen Estes. I learned a lot from him about B5 neurons. He also patiently taught me how to pull the neurons from *Helisoma trivolvis* snails.

I thank all the faculty and staff members at Biology department, especially Ms. LaTesha Warren and Ms. Moneka Jones for their professional assistance. I'd like to appreciate the friendship and supports from all my friends including but not limited to Shian McLeish and Samara Rivers and any other people that I've forgot to mention their name here.

TABLE OF CONTENTS

LIST OF FIGURES

LIST OF TABLES

1 INTRODUCTION

The spike shape is an important factor in neuronal functioning (Ma & Koester, 1995). The size of the spike width determines the calcium influx through voltage-gated ionic channels (Augustine, 1990; Estes *et al.,* 2014). It is shown in the literature that the spike width is positively correlated with the intracellular calcium concentration ($[Ca^{2+}]_i$) (Gillette *et al.*, 1980). The $[Ca^{2+}]_i$ regulates various neuronal processes such as neurotransmitter release, neuronal development, synaptic plasticity, and gene transcription (Berridge *et al*., 2003). For instance, the level of cytosolic calcium is increased in the brains of patients with Alzheimer's disease; the calcium release through ryanodine receptor (RYR) channels of the endoplasmic reticulum (ER) membrane is implicated in this increase (Lopez *et al*., 2008). It is shown that dantrolene, an antagonist of RYR, nearly abolishes memory loss in a mouse model of Alzheimer's disease (Peng *et al*., 2012). It is also known that dantrolene has protective effects on neuronal damages caused by ischemia, hypoxia, seizure, sepsis, and spinocerebellar ataxia (Peng *et al*., 2012; Inan & Wei, 2010).

One of the important effects of changes in $[Ca^{2+}]_i$ is the regulation of neuronal development (Estes *et al*., 2014; Zheng & Poo, 2007). Calcium signaling regulates the growth cone motility in B5 neurons of the fresh-water snail *Helisoma trivolvis* and is determined by the shape of the action potential (Zhong *et al*., 2013; Estes *et al*., 2014; Rehder & Kater, 1992). The key ionic currents required for spontaneous and evoked spiking in B5 neurons are persistent sodium (I_{NaP}), hyperpolarization-activated current (I_H), calcium current (I_{Ca}), and Ca-activated potassium currents including big and small conductances (I_{BK} and I_{SK}). It is shown that the amplitude of I_{SK} and I_{BK} and the voltage of half-activation of I_H can be modulated based on

changes in the level of $[Ca^{2+}]_i$ (Zhong *et al*., 2013; Hagiwara & Irisawa, 1989; Destexhe *et al.*, 1993; Luthi & McCormick, 1998).

The unpublished data from our collaborators, Artinian and Rehder, showed that dantrolene treatment of B5 neurons gradually decreases their firing frequency and eventually silences the neuron. At the same time, dantrolene changes the spike shape. For example, the spike width decreases and the minimum after-hyperpolarization potential (mAHP) becomes more negative. It was shown that dantolene treatment causes a reduction of the persistent sodium current and the hyperpolarization-activated current (h-current). These two currents are important in generating the spiking activity in B5 neurons. Both currents activate in the range of resting membrane potentials. The study of the effects of these ionic currents on spiking properties of B5 neurons would provide us with pivotal information about the dynamics of the neuronal activity.

The biophysical model of B5 neurons can help us to understand the cellular mechanisms that control the spike shape properties such as the spike width and mAHP. The knowledge of neural dynamics gives us qualitative and quantitative predictions about the behavior of the neurons (Cymbalyuk *et al.,* 2002; Barnett & Cymbalyuk, 2014; Barnett *et al.,* 2013; Malaschenko *et al.,* 2011; Shilnikov & Cymbalyuk, 2005; Shilnikov *et al*., 2005). By using the model, we can measure the calcium influx through calcium channels during a single action potential. The correlation between the measured level of $[Ca^{2+}]_i$ and the width of action potential is investigated in the model. This study focuses on two goals: (1) to develop a canonical model of B5 neurons, and (2) to determine the mechanisms by which persistent sodium and h-current affect the spike shape.

2 MATERIALS AND METHODS

2.1 Canonical model of B5 neurons

We developed a biophysical model of identified B5 neurons of fresh water snail *Helisoma trivolvis.* It reproduces the neuronal firing activity under different experimental conditions. The study of single identified B5 neuron in culture provided a plethora of data on its intrinsic electrical dynamics and calcium signaling. First, a preliminary Hodgkin-Huxley-type model of a B5 neuron was developed, which contained the key ionic currents and reproduced the electrical activity of these neurons. The analysis of spiking activity indicated that the main current generating spikes in B5 neurons is calcium current (Artinian *et al*., 2010). Neurons in NMDG saline, which eliminates sodium currents, are silent but still able to generate action potentials during the application of depolarizing injected current. The model exhibited a firing activity of B5 neurons comparable to the activity observed in the experiments (Fig.1).

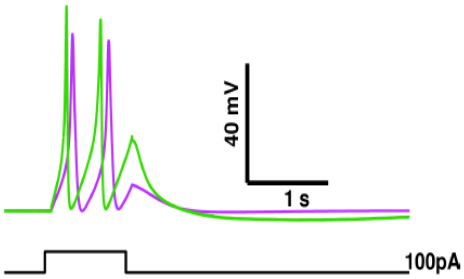

Figure 1: The activity of B5 neurons in NMDG saline. *The 100 pA depolarizing injected current is applied to a silent neuron for 1 s. The green curve shows the experimental data and the pink curve is the model activity. The black line shows the trace of injected current.*

Different methods of optimization such as evolutionary algorithm, gradient descent method, and simplex method were applied in the model to find the best biological parameter set reproducing the firing activity of these neurons. Further enhancement of the neuronal model was obtained by tuning the parameters of ionic currents including I_H and I_{NaP}.

In the second part of this study, we determined the role of I_{NaP} and I_H in forming the spike shape of B5 neurons. Our modeling data supports the notion that the down-regulation of persistent sodium current by reducing its maximal conductance (G_{NaP}) and the removal of the h-current by shifting the voltage of half-activation ($V_{1/2mH}$) to more hyperpolarized values can lead to the recorded change of spike properties. The most prominent changes are decrease of the spike width, the shift of mAHP to more hyperpolarized values, and decrease of the spike frequency. The analysis of ionic gating variables allowed us to study the mechanisms underlying neuromodulation of B5 neurons based on changes in properties of I_{NaP} and I_H. We found a linear correlation between the calcium influx into the cell and the spike properties, such as spike width and spike frequency.

Our Hodgkin-Huxley-type neuronal model of B5 neurons includes ten ionic currents: fast sodium current, I_{NaF}; persistent sodium current, I_{NaP}; delayed rectifier potassium current, I_K; A-type potassium current, I_{Ka}; non-inactivating potassium current, I_{K4}; voltage-gated calcium current, I_{Ca}; calcium-activated potassium currents (small conductance and big conductance), I_{SK} and I_{BK}; hyperpolarization-activated current (h-current), I_H, and leak current, I_L (Appendix). It is based on the model of respiratory neurons of the central pattern generator (CPG) of the pond snail *Lymnaea* (Bungay *et al*., 2009). Three additional currents were added from other sources. The h-current (I_H) was derived from a model of a leech heart (Hill *et al*., 2001; Barnett & Cymbalyuk, 2014), calcium-activated potassium currents (I_{SK} and I_{BK}) were taken from Baxter *et al*. (1999), and non-inactivating potassium current (I_{K4}) were derived from Hille (1991) (Hille, 1991; Baxter *et al*., 1999). The parameters of the full model were tuned to reproduce the experimental activity of B5 neurons (Table A.1). The final model used in the simulations is described in the Appendix section.

All the simulations and analyses were performed using custom-made scripts written in MATLAB (The Mathworks, Inc.). The system of differential equations describing the B5 neuron were simulated using the integration method of backward differentiation formulas (BDF), applying the function ode15s. The real tolerance and absolute tolerance of the integrations were 10^{-9}. The simulated model exhibited stationary states and spiking activity. In order to achieve steady-state spiking activity, the model was integrated for 50 seconds and then the analyses were applied to evaluate the properties of spike shapes. We compared the spike shapes simulated in the model with intracellular experimental recordings (Dr. Rehder's lab, Georgia State University, Atlanta, GA, USA) and tuned the model parameters to match the spike properties such as amplitude, spike width, inter-spike interval, and threshold, peak of spike, and mAHP.

2.2 The definition of the spike width

The spikes were characterized by the width at the threshold voltage of action potential. We determined the threshold by applying the same procedures to both experimental and modeling data. The only distinction was that the experimental data were filtered to remove noise. Experimental voltage traces were low-passed filtered by using eighth-order Bessel filter (Sekerli *et al*., 2004). The Bilinear transformation was used to transform an analog Bessel filter to digital counterpart with cutoff frequency fixed to 1250 Hz (Sekerli *et al*., 2004). The filtering procedure didn't noticeably change the spike shape. In order to determine the threshold voltage, we used the first derivative of membrane potential (dV/dt). We calculated dV/dt by applying the central difference method provided in MATLAB. The phase-plane plot, dV/dt versus membrane potential (V), provides insight into the dynamics of spiking activity (Guttman *et al*., 1980; Butera *et al*., 1995; Sekerli *et al*., 2004). The spike threshold was estimated by plotting the rising section of the derivative in the phase-plane, as the voltage at which the dV/dt equals to 3% of its

maximum (V_{th}) (Fig. 2A,B). The measured spike width at V_{th} was used as one of the characteristics to match through the optimization.

2.3 Optimization of the parameters of ionic currents in the model

Different optimization techniques including Nelder-Mead simplex method, evolutionary algorithm, and gradient descent method were applied to tune the parameters of ionic currents. In each optimization routine from three to ten parameters where selected to be optimized. A cost function was developed to assess the mismatch of the model and experimental data. During the optimization, the value of the selected parameters were varied to minimize the cost function.

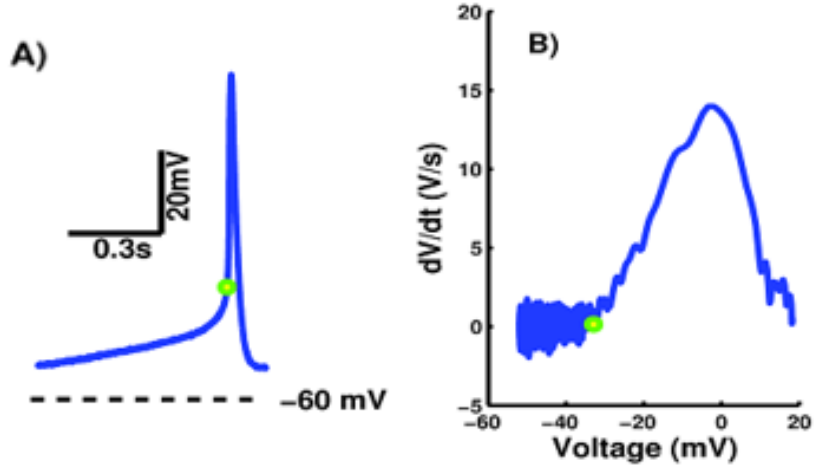

Figure 2: Definition of the spike threshold*. The threshold voltage is determined by analysis of the voltage derivative and marked by a green circle. The V_{th} is equal to -33.5 mV.* ***A)*** *An example of action potential in control.* ***B)*** *The positive region of the membrane potential derivative (derivative of the depolarizing part of action potential) versus membrane potential.*

We defined two types of cost functions for optimization of the selected characteristics. We used each of these cost functions separately in our optimization routines. (1) The first cost function was defined on the basis of comparison between the voltage traces obtained in the model and in the experiment. For this reason, we aligned the model and experimental spikes placing the maximum voltages at time zero. As the inter-spike intervals were not exactly the

same, we created a window between the rising and decaying parts of action potential to compare the corresponding voltages between the two spikes. We chose the smallest depolarizing and repolarizing parts between the action potentials, and then created the window based on that time range. The sum of the absolute values of the voltage trace difference between the two action potentials in the created window was used as the cost function. (2) The other cost function was defined by comparing the spike shape characteristics in the model and the experiment. The values of dV/dt at the two key points on the phase-plane of a single spike refer to maximum and minimum of the dV/dt, the threshold, peak of spike, and mAHP of the action potential were considered in calculating the cost function. The other characteristics of the spike shape such as spike width, inter-spike interval, and the amplitude were also calculated in the model and the experiment. We measured the absolute value of the difference between the mentioned characteristics of action potential in the model and the experiment. The results were normalized in a way that each of the calculated difference values had the same effect on optimization of the spike's characteristics. The second cost function calculates the sum of the normalized values. The canonical model was obtained by applying the optimization methods for several rounds until the model exhibited a minimal cost function value and could closely reproduce the voltage trace under given conditions.

2.4 Effects of the removal of I_H and I_{NaP} on the spike shape

We investigated the changes of the spike shape during spiking activity exhibited in the model under two applied conditions: (1) blockade of the h-current and (2) reduction of the persistent sodium current. The latter was obtained by decreasing the maximal conductance of the persistent sodium current. To remove the h-current in the model, two methods were used. First, the maximal conductance of the h-current was set to zero. In this case, the rest of the ionic

current parameters in the model were optimized as described in section 2.2. We compared the spike shape between the model and the experiment in control condition and under ZD7288 treatment, a blocker of the h-current. Second, we modeled the removal of the h-current by shifting its voltage of half-activation ($V_{1/2mH}$) towards more hyperpolarized potentials in our canonical model.

One of the important consequences of spiking is the calcium influx into the cell caused by each action potential. The relation of the spike width and calcium influx was assessed as $V_{1/2mH}$ was systematically shifted to different voltages. We evaluated the total calcium influx during a single spike, which is determined by the interval between the moment when the membrane potential crosses the threshold and the moment when it reaches the mAHP. The equation 16 in the Appendix was used to calculate the calcium influx for different $V_{1/2mH}$.

The cellular mechanisms that control the spike shape were identified in the model. We investigated the most influential variables controlling the changes in the spike width and mAHP.

3 RESULTS

3.1 H-current removal mimics the dantrolene effects on spike shapes

The ionic currents essential for spontaneous and evoked spiking in B5 neurons are persistent sodium current (I_{NaP}), h-current (I_H), calcium current (I_{Ca}), and calcium-activated potassium current (I_{SK} & I_{BK}) (Artinian *et al.*, 2012). The two inward currents, I_{NaP} and I_H, play special roles in determining the spike shape of B5 neurons. The experimental data showed that dantrolene treatment reduced the persistent sodium current and inhibited the h-current. In the consequence of applying dantrolene, the spike shape changed so that the spikes became larger in amplitude and narrower in width. The peak of spike after dantrolene treatment slightly decreased

and the increase in the spike amplitude was solely caused by the shift of mAHP towards more negative voltages. The peak of the spike did not change significantly for spikes before and after dantrolene treatment. Similar changes in spike shapes were reported after inhibition of the h-current by ZD7288 treatment.

To model the effects of ZD7288 treatment, we started with our canonical model and removed the h-current by setting its maximal conductance to zero (G_H = 0 nS) (Fig. 3A,B). The spike shape properties were matched closely with the experimental data by applying optimization algorithms. In accordance with the experimental results, the spike width was reduced from 40.1 ms in control to 27 ms after the blockade of the h-current. Similarly, the simulations showed a reduction of spike width by ~16%, from 40.7 ms in control to 34.3 ms after the removal of the h-current. Furthermore, the application of ZD7288 shifted the mAHP from -52.6 mV to -57 mV in experiment. The model exhibited a similar reduction of mAHP from -52.6 mV in control to -55 mV after the h-current was removed (Fig. 3A,B).

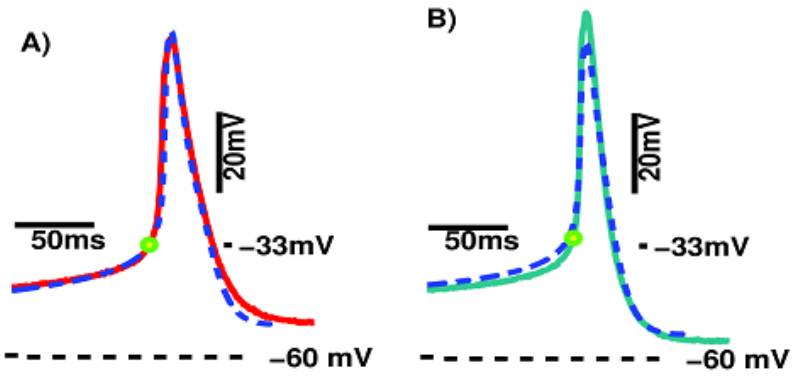

Figure 3: Spike shape in control and after ZD7288 treatment in the model and the experiment. *The dark blue dashed lines represent the spikes exhibited by the model and the solid curves (red and green) present the experimental data. The shape of an action potential before and after ZD7288 treatment is plotted in (A) and (B), respectively. The green circles mark the threshold voltage.*

The peak of spike in the experiment during dantrolene treatment decreased by 1.5 mV. In our model, the decrease in the peak of spike is qualitatively in agreement with the dantrolene experiment. Therefore, we overlook the mismatch of the peak of spike between the model and experiment under ZD7288 treatment and give priority to the data obtained from dantrolene treatment. However, the changes in the spike width and mAHP were well matched in the experiment and the model after the removal of the h-current, which these changes on the spike shape were also observed in dantrolene experiment as well.

3.2 Control of the h-current by variation of $V_{1/2mH}$

The voltage of half-activation of the h-current is controlled and activated by the intracellular calcium concentration ($[Ca^{2+}]_i$) (Destexhe *et al.*, 1993; Hagiwara & Irisawa, 1989). Calcium stores are one of the main sources of regulation of the intracellular calcium concentration. Dantrolene, the specific inhibitor of ryanodine channel-mediated calcium release from intracellular stores, inhibited the h-current and continuously decreased the spike width and lowered the mAHP in B5 neurons. We manipulated the amount of the h-current in the model by shifting $V_{1/2mH}$ to more hyperpolarized values. This way the h-current was removed from the system as it would activates only at voltages outside the range of variation of voltage during the spike. In this section, we investigated the effect of the h-current on properties of the action potentials by systematically shifting its voltage of half-activation from -110 mV to +20 mV. This procedure provides us information of the correlation between various spike properties such as the spike width, mAHP, and the spike frequency. We compared the trend of changes of the spike properties in the model as we shifted the $V_{1/2mH}$ towards more hyperpolarized values with the corresponding results after dantrolene treatment.

3.2.1 Spike width decreased at more hyperpolarized values of $V_{1/2mH}$

We analyzed the changes on spike shape during spiking activity in the canonical model of B5 neurons associated with the down-regulation of the h-current by shifting its voltage of half-activation ($V_{1/2mH}$) to more hyperpolarized voltages. Similar to the effects of the blockade of the h-current by setting its maximal conductance to zero, the model showed a reduction of the spike width and a shift in mAHP to more hyperpolarized values as we shifted $V_{1/2mH}$ from depolarized value +20 mV to hyperpolarized value -110 mV (Fig. 4,5). At $V_{1/2mH}$ equals -110 mV, the spike characteristics were saturated. The system produced steady-state spiking activity for all the mentioned values of $V_{1/2mH}$, from +20 mV to -110 mV.

The spike width correlated non-linearly with $V_{1/2mH}$ and had a maximum of 42.1 ms at $V_{1/2mH}$ of -48 mV (Fig. 4). The shift of $V_{1/2mH}$ from values of -48 mV to -110 mV decreased the spike width by 18%, from 42.1 ms to 34.5 ms. In contrast, the spike width values changed in opposite direction as we shifted $V_{1/2mH}$ from depolarized values of +20 mV to -48 mV. The width of spikes increased by 12%, from 37.5 ms to the maximum value 42.1 ms. It should be noted that the most depolarized values of $V_{1/2mH}$ investigated were outside of the physiological range.

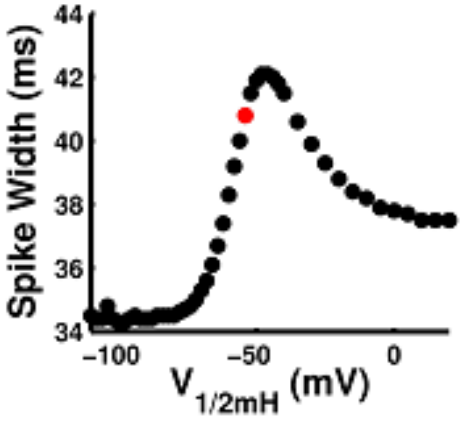

Figure 4: Dependence of spike width on $V_{1/2mH}$. *The red dot represents the canonical value of $V_{1/2mH}$. The graph has a maximum at 42.1 ms at -48 mV.*

3.2.2 The Dependence of the minimum after-hyperpolarization potential on $V_{1/2mH}$

Dantrolene treatment increase the mAHP by shifting it to more negative values. In the model, we investigated whether similar changes could be caused by shifting $V_{1/2mH}$. As we changed $V_{1/2mH}$ in the same range of -110 mV to +20 mV, the mAHP increased from -55.0 mV to more depolarized value of -49.6 mV. We obtained a non-linear correlation between the mAHP and value of $V_{1/2mH}$ (Fig. 5). The mAHP is saturated at -55.0 mV for the $V_{1/2mH}$ values below -86 mV. It indicates that the h-current is not participating in the spiking dynamics for $V_{1/2mH}$ values smaller than -86 mV. As we increased $V_{1/2mH}$ from -86 mV to more depolarized values, the mAHP also increased to more depolarized values at two different rates. The mAHP changed rapidly for $V_{1/2mH}$ values between -86 mV and -48 mV, and slowly $V_{1/2mH}$ values more depolarized than -48 mV.

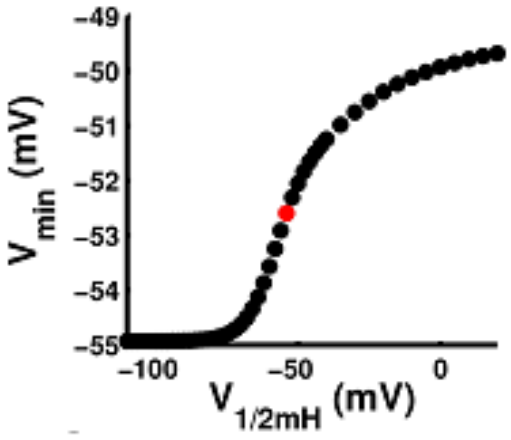

Figure 5: Dependence of the minimum after-hyperpolarization potential on $V_{1/2mH}$. *The red dot represents mAHP for the canonical value of $V_{1/2mH}$.*

3.2.3 Linear correlation of the spike width and the minimum after-hyperpolarization potential

We next investigated the relationship between the changes in the spike width and the mAHP as $V_{1/2mH}$ was shifted between -110 mV to +20 mV. Figure 6 shows a maximum of the spike width at 42.1 ms with mAHP equals -51.8 mV, which corresponds with $V_{1/2mH}$ equals -48 mV (Fig. 4,6). We split the curve into two parts, and then fitted each part with linear functions. The slope of the fitted line of the rising part of the curve was 2.5 ms/mV. Over this part of the curve, the spike width increased from 34.5 ms to 42.1 ms while the mAHP changed from -55 mV to -51.8 mV. Similarly, the decreasing part fitted with a linear function that had a slope of -2.6 ms/mV. Here, the spike width decreased from 42.1 ms to 37.5 ms while the mAHP increased to -49.6 mV. The rate of change of the spike width is slightly higher for the decreasing part than for the rising part of the curve.

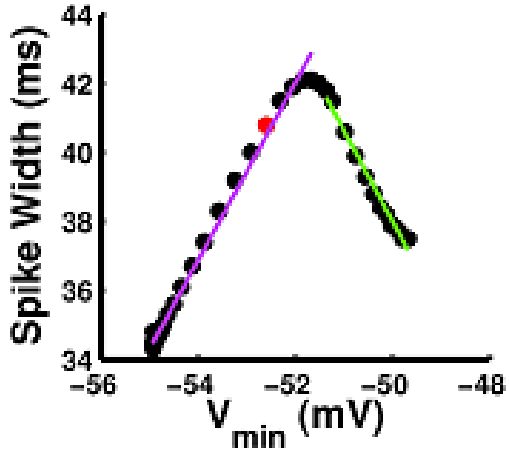

Figure 6: Dependence of spike width on minimum after-hyperpolarization potential under variation of $V_{1/2mH}$. *The black dots present the spike width and mAHP as $V_{1/2mH}$ is shifted from -110 mV to +20 mV. The curve creates a maximum spike width of 42.1 ms corresponding to mAHPof -51.5 mV. The graph is analyzed in two parts: before and after the maximum and each part is fitted with a linear function. The slopes of the rising and declining parts of the curve are 2.5 ms/mV (the pink line) and -2.6 ms/mV (the green line), respectively.*

The linear correlation between spike width and the mAHP was also tested in the experiment in control condition and during dantrolene treatment (Fig. 7). Similar to the result obtained from the model, the experimental data demonstrated a linear correlation between the spike width and the minimum voltage (Fig 6, 7A). In the experiments, the spike width decreased from 28 ms to 19 ms as mAHP moved to more hyperpolarized values from -53.2 mV to -59.5 mV due to dantrolene treatment. The slope of the line fitted to the experimental data was ~1.6 ms/mV. Although it was smaller than the slope obtained for the model, it was remarkable to confirm the prediction. Dantrolene treatment also decreased the spike frequency from 1 Hz to 0.15 Hz, and then neuron became silent (Fig. 7B). The spike width and the spike frequency were also correlated linearly with a fitted slope of 9 ms/Hz.

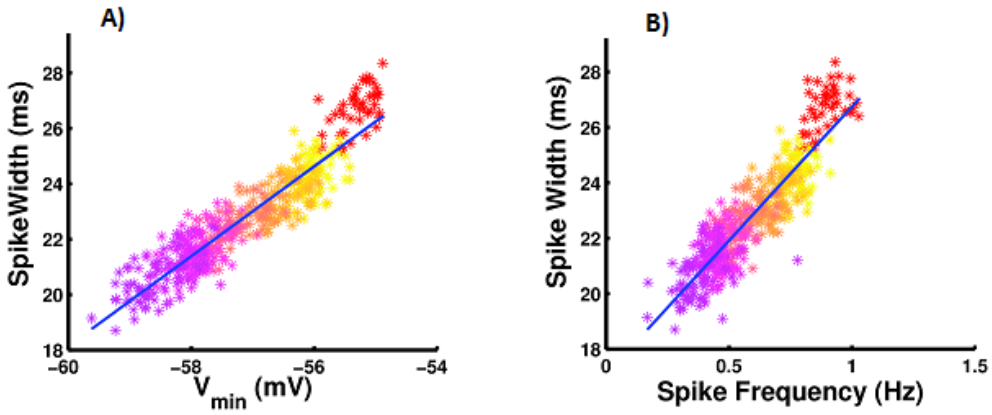

Figure 7: The properties of action potentials of experimental data in control and after treatment with dantrolene. *The stars represent the spike width, minimum voltage and frequency for each action potential. The red stars mark the spike properties in control neurons. Yellow to purple stars are showing the changes in spike properties over time upon dantrolene application.* ***A)*** *The fitted line with slope of 1.6 ms/mV describes the correlation of the changes in spike width and mAHP.* ***B)*** *The spike width is decreasing in a linear fashion as spike frequency decreased. The slope of the line is 9 ms/Hz.*

In summary, shifting the voltage of half-activation of the h-current to more hyperpolarized values showed similar effects on spike shape as those caused by dantrolene

treatment. Removal of the h-current by shifting $V_{1/2mH}$ to more hyperpolarized values decreased the spike width and shifted the mAHP to more negative voltages. The model showed non-linear dependencies of both spike width and mAHP based on variation of $V_{1/2mH}$. However, the spike width linearly correlated with the mAHP, in both model and experimental data. The changes in the spike caused by the removal of h-current were further studied in the model and were compared to experimental result.

3.2.4 The regulation of spike properties

The application of dantrolene noticeably decreased the frequency of spiking activity of B5 neurons before it silenced the neurons. The question is how the spike width is correlated with the spike frequency during dantrolene treatment. Since dantrolene treatment removed the h-current, we further investigated the changes of spike frequency in the model as $V_{1/2mH}$ was shifted to more hyperpolarized values. The spontaneous spike frequency was calculated as the inverse of the time interval between maximum voltages of two consequent spikes. The spike frequency decreased non-linearly as $V_{1/2mH}$ was shifted to more negative values. The frequency was saturated at the value of 0.7 Hz for $V_{1/2mH}$ voltages below -86 mV (Fig. 8). The spike frequency non-linearly increased, from 0.7 Hz to 7.3 Hz, for $V_{1/2mH}$ values more depolarized than -86 mV up to +20 mV. The spike frequency in the canonical model was 2.3 Hz at $V_{1/2mH}$ equals -54.5 mV.

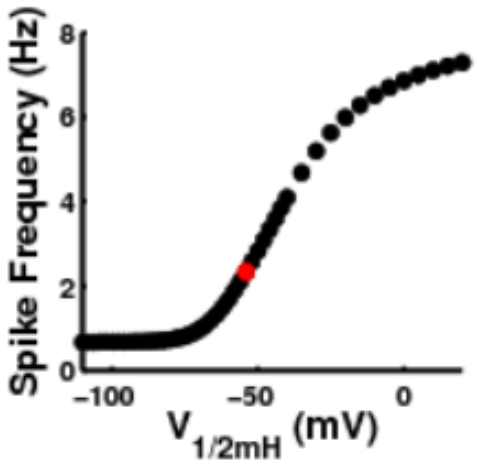

Figure 8: Spike frequency versus $V_{1/2mH}$. *The red dot represents the canonical value. The frequency changed from 0.7 Hz to 7.3 Hz. The spike frequency is saturated at 0.67 Hz for $V_{1/2mH}$ smaller than -86 mV.*

The graph of spike width and spike frequency exhibits a maximum frequency at 3.1 Hz with recorded spike frequencies varying between 0.7 Hz to 7.3 Hz (Fig. 9). The maximum point of this curve corresponds to the maximum point obtained in Figure 4 at $V_{1/2mH}$ equals -48 mV (Fig. 4,9). We characterized the curve by splitting it into two parts and fitted each part with a linear function. The rising part of the curve corresponds to the physiological changing range of $V_{1/2mH}$ and fitted to a line with a positive slope of 3.6 ms/Hz. Similarly, in the dantrolene experiment, the spike width linearly correlated with the spike frequency.

All together, the application of dantrolene in the experiment showed a linear correlation between the spike width and spike frequency. In the model, we reproduced the dantrolene effect on the h-current by shifting $V_{1/2mH}$ from its physiological range towards more hyperpolarized values. This blocked of the h-current resulted in a qualitative similar linear correlation between the spike width and spike frequency.

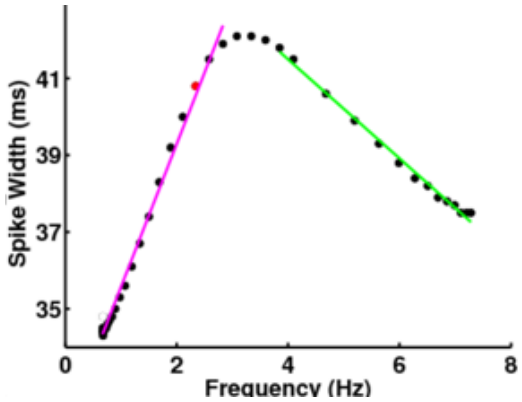

Figure 9: The dependency of spike shape properties on spike frequency under variation of $V_{1/2mH}$. *The red dot corresponds to the canonical value of $V_{1/2mH}$ for spike frequency 2.3 Hz. The curve of spike width and frequency has the maximum of 42.1 ms at spike frequency of 3.1 Hz. The curve can be divided into two linear parts with positive slope of 3.6 ms/Hz and negative slope of -1.3 ms/Hz.*

3.3 Linear correlation of calcium influx, spike frequency, and spike width

The spike shape determines the level of intracellular calcium concentration (Estes *et al.*, 2014). The spike frequency positively correlates with the $[Ca^{2+}]_i$ (Estes *et al.*, 2014). In our model, the removal of the h-current led to a reduced spike width and an increase in the inter-spike interval (ISI). We investigated the calcium influx through calcium channels as $V_{1/2mH}$ was shifted from -48 mV to -110 mV. The calcium influx was calculated at each value of $V_{1/2mH}$. We fixed the value of the cell volume to 7.9 nL (Table A.2), and calculated the calcium concentration in this volume depending on the calcium influx into the cell for 10 s. The results showed that this intracellular calcium concentration linearly correlated with the spike frequency and increased by 1020 nM, from 380 nM to 1400 nM, as the spiking frequency increased from 0.7 Hz to 3.1 Hz. The slope of the line is 431 nM/Hz in the model (Fig. 10A), which is similar to the slope of the fitted line between the firing frequency and growth cone calcium concentration of B5 neurons obtained in the experimental data in Estes *et al.* paper.

We also calculated the calcium influx during a single spike, i.e. during the time interval from the moment when the membrane potential crosses the threshold voltage to the moment when it reaches the mAHP. For the spike broadening of 8 ms, the $[Ca^{2+}]_i$ due to the calcium influx increased by 22 nM, from 56 nM to 78 nM (Fig.10B).

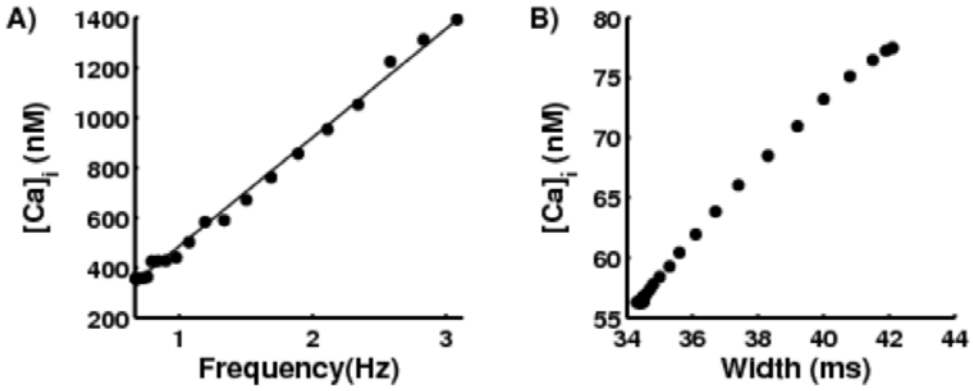

Figure 10: The relation of the calcium concentration and the spike properties*. The black dots represent the average value of intracellular calcium concentration due to calcium influx calculated for a 10 s interval in (A) and during a single spike in (B).* ***A)*** *The slope of the fitted line is 431 nM/Hz.* ***B)*** *The calcium influx of a single spike is positively correlated with the spike width.*

3.4 The inactivation variables of three inward currents at the threshold voltage controlled the spike shape

In the model, we investigated the specific cellular mechanisms, which control the spike width and mAHP. Our goal is to identify the key gating variables of ionic currents that govern the changes of these two properties of the spike shape. We analyzed the spike shapes exhibited in the model in response to perturbation of the gating variables, one at a time. We compared two models, which differ only in one parameter value: the voltage of half-activation of the h-current ($V_{1/2mH}$). We considered the two values of this parameter that would create the largest spike width difference. We called these two models: the wide-spike model and the narrow-spike

model. We tested whether reset of the original value of a variable in one model, to the initial value of the same variable in the other model, could reproduce the spike shape of the latter model. For example, would the initial value of the inactivation variable of the calcium current of the wide-spike model, plugged as the initial value of the same variable into the narrow-spike model, cause the latter to produce a wide spike?

As mentioned before, the model exhibited steady-state spiking activity for all analyzed values of $V_{1/2mH}$ in the range between -110 mV and +20 mV. The narrowest and the widest spike widths were recorded in the model at $V_{1/2mH}$ -88 mV and -48 mV, respectively (Fig. 4). The spike width of the narrow-spike model and the wide-spike model were 34.3 ms and 42.1 ms, correspondingly. The perturbation is applied to each variable at certain points on the action potential. For example, the spike threshold was one of the points where we applied the perturbation. At the spike threshold, the value of one variable in one of the selected models (e.g. narrow-spike model) was exchanged with the value of the same variable of spiking activity in the other model (e.g. wide-spike model). Then, we measured the width of the first spike generated after the perturbation and calculated the difference with the spike width of the same model before perturbation. We assumed that perturbation of one or a group of variables in one model could generate one action potential with the spike width of the other model. We calculated the spike width difference obtained from one model in unperturbed condition and after the perturbation. We formalized the percentage of this difference relative to the largest spike width difference obtained from the two models in their unperturbed conditions. We called this percentage an effective value. Higher percentages specify that the value of the perturbed spike width difference is closer to the maximal spike width difference obtained from unperturbed conditions. In other words, the value of 100% represents the exact match of the spike width after

the perturbation in one model (e.g. wide-spike model) with the spike width of the other model in its unperturbed condition (e.g. narrow-spike model).

Our B5 model contains 11 activation and inactivation gating variables along with the voltage variable. The exchange of variables at the spike threshold didn't change the depolarizing part of the spike, and it was the same in control and after the perturbation (Fig. 11). The spike width was only changed based on the changes in the repolarization part of the action potential. The perturbation of gating variables of outward currents at the threshold showed an effective value less than 1%. Similarly, perturbation of the activation variables of inward currents showed slight changes in the spike width and obtained an effective value of less than 1%. Distinctly, perturbation of the inactivation variables of three inward currents, namely: fast sodium, persistent sodium and calcium currents exhibited high percentage corresponding to a significant change in spike width. The effective values were slightly different depending on which model was perturbed. The perturbation of the inactivation variables of fast sodium, persistent sodium and calcium currents in the narrow-spike model resulted in effective values of 22%, 11% and 47%, respectively, while the wide-spike model showed effective values of 37%, 28% and 71%. Since perturbation of a single variable could not completely reproduce the spike width from one perturbed model to the other unperturbed model, we analyzed the changes in spike width by simultaneously perturbing a group of variables. We chose a combination set of two or three variables out of the inactivation variables of these three inward currents. The perturbation of a combination of two variables indicated higher percentages than the effective values obtained by perturbation of only one variable. However, the joint perturbation of all three variables resulted in the highest percentage and the significant change in the spike width (Fig. 11). The effective value obtained by perturbing all three variables together was not equal to the sum of the effective

values obtained from the perturbation of single variables. The synergy of perturbation of all three variables resulted in an effective value of 113.5% in the narrow-spike model and 103% in the wide-spike model. It suggested that the joint perturbation of inactivation variables of these three inward currents in one model over-adjusts the spike width from its unperturbed value in the other model.

As it shows in Figure 11E, the repolarization part of the action potential in the perturbed wide-spike model and the unperturbed narrow-spike model matched well with each other (Fig. 11E, pink to dashed red). Similarly, applying the perturbation on the wide-spike model reduced the spike width, and the repolarization part of action potential matched the one in the unperturbed narrow-spike model (Fig. 11E, blue to dashed black).

Since the outward currents are mostly activated at more depolarized potentials, we investigated how the variables at the peak of spike are controlling the spike width. We applied the similar perturbation procedures on each of the variables at the peak of spike, one at a time. However, at the peak of spike, the gating variables of outward currents showed an effective value less than 1%. These result suggest that gating variables of outward currents did not govern the spike width. In turn, the inactivation variables of the inward currents affected the spike width. The results are shown in Table 1.

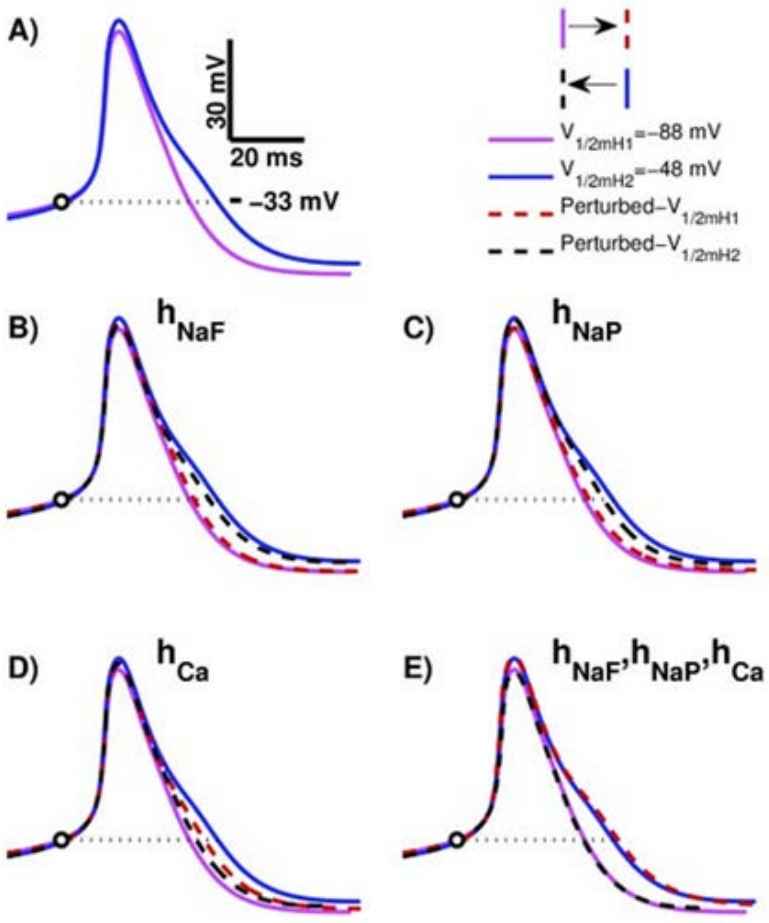

Figure 11: Spike shapes in control and after perturbation applied at the spike threshold. *The pink and the blue curves represent the spike shape in control at $V_{1/2mH}$ -88 mV (narrow-spike model) and -48 mV (wide-spike model), respectively. The graph shows the changes in spike shape induced by perturbation of the inactivation variables of the three inward currents: fast sodium (B), persistent sodium (C), calcium (D) currents, and the all three inactivation variables together (E) at the threshold. The circle and the dotted line mark the threshold voltage. The dashed curves represent the perturbed spike shapes. In perturbation, we exchanged the value of inactivation variables between the two models. The perturbation of the wide-spike model (blue) decreases the spike width (black dashed curve). The perturbation of the narrow-spike model (pink) increases the spike width (red dashed curve). The spike width perfectly matched in two models based on the perturbation of the all three variables simultaneously (E).*

Table 1. The effects of the perturbation at the peak of spike on the spike width

	Spike Width	
Variables	*Wide-spike Model*	*Narrow-spike Model*
h_{NaF}	37%	23%
h_{NaP}	24%	12%
h_{Ca}	64%	44%
h_{NaF},h_{NaP},h_{Ca}	98%	98%
m_h	<1%	<1%
other variables	<1%	<1%

3.5 The activation of the h-current at the minimum after-hyperpolarization potential controls the spike width and minimum after-hyperpolarization potential

At mAHP, we applied the same analysis of the perturbation of the variables described above. The results showed that none of the gating variables except for the activation of the h-current and the voltage had an effective value larger than 1% on the spike width and mAHP.

First, we analyzed the difference of mAHP between control and perturbed spikes. The perturbation of the activation variable of the h-current noticeably changed the mAHP. The larger values of the activation variable of the h-current shifted the mAHP to more depolarized values. The effective values were different between the two models. The perturbation of the narrow-spike model and the wide-spike model yielded effective values of 74% and 53%, respectively.

The perturbation of voltage distinctly affected the mAHP. The effects differed between the two models. The perturbation of the narrow-spike model did not affect the mAHP, while the perturbation of the wide-spike model shifted the mAHP to more depolarized voltages with an effective value of -33%. The minus sign represents that the mAHP was changed in the opposite direction of the value measured in the original model.

Second, we concluded that the perturbation of the same two variables at mAHP controlled the spike width. The rest of the ionic gating variables had an effective value of less

than 1%. The perturbation of the voltage generated different effective values between the two models. The spike width was affected by only less than 1% as the voltage was perturbed in the narrow-spike model. However, the perturbation of the wide-spike model increased the spike width with an effective value of -52%. On the other hand, the activation variable of the h-current switched the value of the spike width between the two models. The effective values obtained from the perturbation of the narrow-spike model and the wide-spike model were 86% and 47%, respectively. The results suggested that at mAHP the activation of the h-current governed the changes in the spike width. Based on our observation, we found in the model that the variables of inward currents govern the changes in spike width.

3.6 The paradoxical effect of the inactivation variable of inward currents on the minimum after-hyperpolarization potential

At the threshold, we also examined how the perturbation of ionic gating variables would affect mAHP. The same approach was used here to find the most effective variables controlling mAHP. Similar to the previous section, we evaluated the effect of perturbation by calculating the percentage of mAHP difference in one model between control and after the exchange-perturbation relative to the maximal mAHP difference between the two models in their original conditions. At the threshold voltage, the perturbation of the inactivation variable of the three inward currents and also the activation variable of the h-current strongly affect the value of mAHP. We obtained different effective values for each of the variables of the mentioned inward currents depending on which model was perturbed. The narrow-spike model showed effective values of 3%, 16%, 32%, and 37% due to perturbation of the inactivation variables of fast sodium, persistent sodium, calcium currents, and activation variable of the h-current, respectively, while the perturbation of these variables in the wide-spike model caused the

effective value of 9%, 25%, 43%, and 46%, respectively. The rest of the variables had a negligible effect of less than 1% on mAHP.

Generally, the removal of inactivation of inward currents determines more hyperpolarized values of mAHP. In our results, at the threshold voltage, the larger value of inactivation variables of the three inward currents determined more depolarized values of the mAHP. In other words, removal of the inactivation of the inward currents shifted the mAHP to more depolarized values. To explain this paradox, we compared the value of these variables at three points on the spike: threshold, peak of spike, and mAHP as$V_{1/2mH}$ was shifted to different values.

3.7 Inactivation of the inward currents during the inter-spike interval

We compared the values of the inactivation variables of fast sodium, persistent sodium, and calcium currents as $V_{1/2mH}$ was shifted from -48 mV to -110 mV. The curves of the variables at the threshold and peak of spike were congruent to each other (Fig. 12). At the threshold and at the peak of spike, the values of these variables monotonically decreased as $V_{1/2mH}$ was shifted to more hyperpolarized values. In contrast, at mAHP, the values of the three variables monotonically increased as $V_{1/2mH}$ was shifted down.

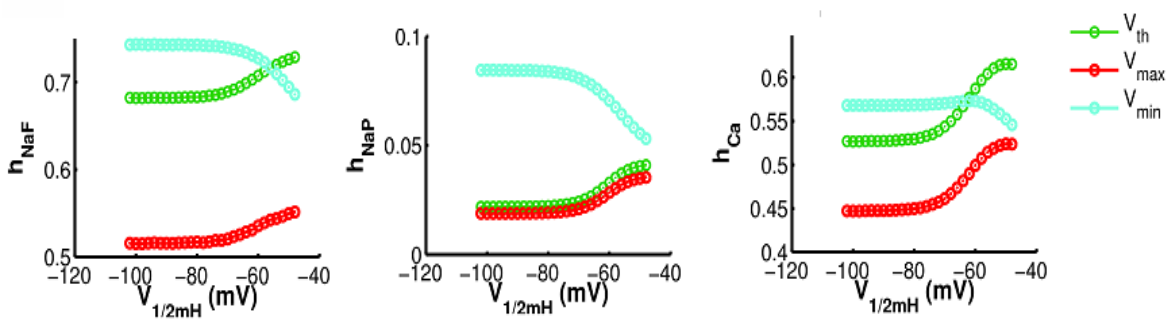

Figure 12: Inactivation variables of three inward currents at different reference points on spike under variation of $V_{1/2mH}$. *The circles show inactivation variables of the three inward currents at the three points of the spike: threshold (green), peak of spike (red), and mAHP (blue)*

as we shift $V_{1/2mH}$ from -110 mV to -48 mV. The V_{min}, V_{max}, and V_{th} represent the mAHP, peak of spike and spike threshold, respectively.

The curves of the inactivation variables at the spike threshold and at mAHP crossed each other at a certain value of $V_{1/2mH}$. This $V_{1/2mH}$ equals -56 mV and -62 mV for the inactivation curves of fast sodium current and calcium current, respectively. It suggests that the activation of the h-current determines the value of these variables.

The spike frequency is controlled by the activation of the h-current; it decreases as $V_{1/2mH}$ was shifted towards more negative values. At the threshold and peak of spike, the inactivation variables of inward currents negatively correlated with the ISI. In contrast, at mAHP, larger ISI corresponds to greater values of the inactivation variables. These results indicated that the inward currents are relatively more inactivated at the threshold and the peak of spike for larger ISI.

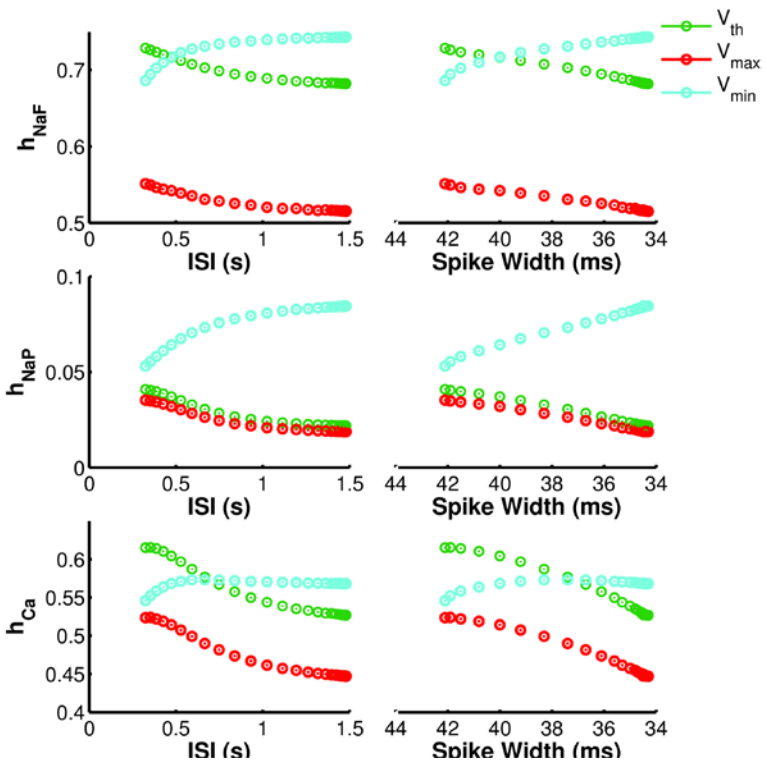

Figure 13: The dependence of the inactivation variables of three inward currents at three reference points of a spike on ISI and on the spike width. *The blue, green and red circles are inactivation variable values at mAHP, spike threshold, and peak of spike, respectively. V_{min} is the*

mAHP. The curves of h_{NaF} at mAHP and at threshold cross each other at an ISI of 0.5 s and a spike width of 40 ms, and the intersection point for h_{Ca} was at an ISI of 0.7 Hz and a spike width of 37.4 ms.

However, at mAHP, the variables are smaller for large values of ISI, where the spikes have more hyperpolarized mAHP (Fig. 13). The spike width was also controlled by the activation of the h-current, and it decreased as $V_{1/2mH}$ was shifted from -48 mV to -110 mV. We showed that the ISI and the spike width are negatively correlated, so that larger ISI is associated with narrower spike width. We also observed that at the threshold and at the peak of spike, the inactivation variable of the three inward currents obtained smaller values for larger ISI.

3.8 Reduction of the persistent sodium current decreases the spike width and minimum after-hyperpolarization potential in B5 neurons

Persistent sodium current plays a special role in spontaneous and evoked spiking in B5 neurons (Artinian et al., 2012). Experimental results of B5 neurons showed that application of dantrolene inhibits the persistent sodium current by ~76%. In the model, we examined the effect of persistent sodium current on spike shape properties by reducing its maximal conductance (G_{NaP}) from 150 nS to zero.

We fixed all the parameters including $V_{1/2mH}$ to their canonical values and then systematically reduced G_{NaP}. The removal of the persistent sodium current decreased the spike width by 22%, from 44.7 ms to 34.8 ms, based on a fitted quadratic function: $f(x)=(7.8\times 10^{-5})x^2+0.025x+20.4$ (Fig. 14A). The mAHP shifted to more hyperpolarized values, from -51.5 mV to -54.5 mV, by the reduction of G_{NaP} (Fig. 14B). We analyzed the correlation of spike width and mAHP as G_{NaP} was decreased in the model. Here, the changes of the spike width based on a shift of mAHP to more hyperpolarized values was described by a quadratic function: $f(x)=0.63x^2+71.2x+(2\times 10^3)$ (Fig. 14C).

We further investigated the effect of G_{NaP} on the spike frequency. The spike frequency slightly decreased from 2.4 to 2.1 Hz for smaller values of G_{NaP} (Fig. 14D). Figure 14E shows the correlation between the spike width and spike frequency as the persistent sodium is decreased. The spike width decreased noticeably by 9.9 ms as frequency decreased by only 0.29 Hz (Fig. 14E). We also analyzed how the mAHP and spike frequency correlated with each other based on the removal of the persistent sodium current. The mAHP shifted towards more hyperpolarized values continuously by 3 mV, from -51.5 mV to -54.5 mV, as spike frequency changed from 2.4 Hz to 2.1 Hz (Fig. 14F).

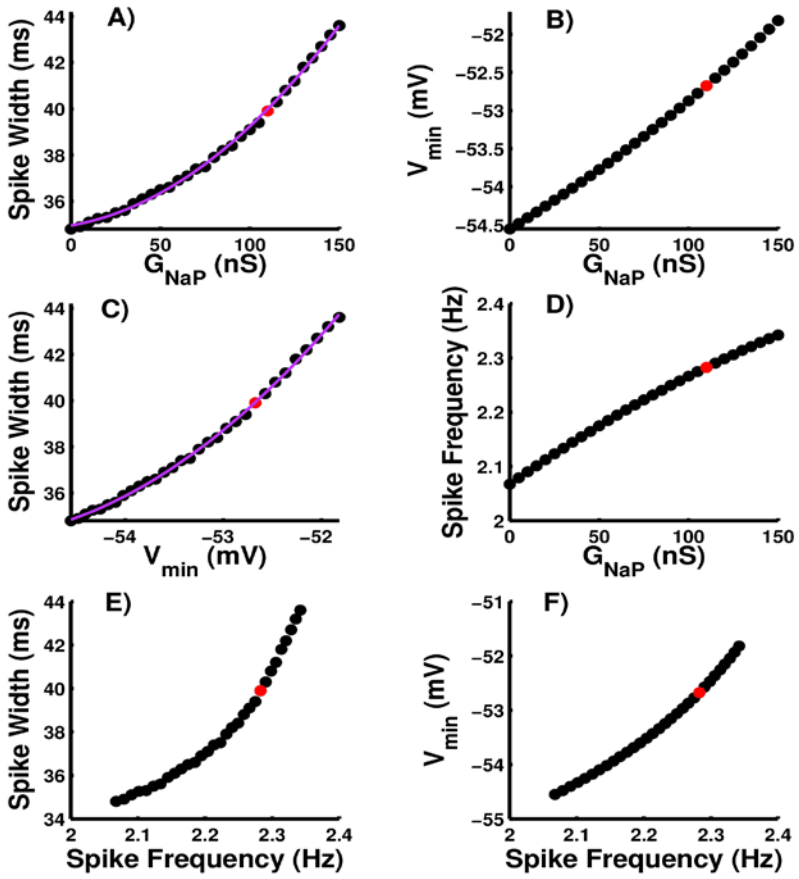

Figure 14: Correlation of spike properties and the persistent sodium current. *The black dots represent the spike properties for each value of G_{NaP}. The red dots mark the canonical value of G_{NaP}. A) The spike width is fitted with a quadratic function:* $f(x)=(7.8\times 10^{-5})x^2+0.025x+20.4$ *. B) The graph represents the mAHP as G_{NaP} is*

decreased. C) The spike width versus mAHP for changing value of G_{NaP}, which is fitted with a quadratic function: $f(x)=0.63x^2+71.2x+(2\times 10^3)$. D) The spike frequency is almost linearly dependent on G_{NaP}. E) The spike width grows with spike frequency. F) For higher spike frequencies, the mAHP shifted towards more depolarized voltages.

4 DISCUSSION

4.1 The significance of spike shape in neuronal processes

In neuronal networks, neurons interact by producing electrical spikes. The spike shape affects neuronal dynamics and efficiency of information transmission (Augustine, 1990; Ma & Koester, 1995), determines the metabolic efficiency (Hasenstaub *et al.*, 2010; Carter & Bean, 2009) and the magnitude of calcium influx, and can govern the intracellular calcium concentration ($[Ca^{2+}]_i$) (Gillette *et al.*, 1980; Augustine, 1990; Estes *et al.*, 2014). In turn, the level of free cytosolic calcium controls a variety of neuronal processes including homeostatatic regulation of activity (Liu *et al.*, 1998; Marder & Prinz, 2002; Gunay & Prinz, 2010), neurotransmitter release (Augustine, 1990; Sabatini & Regehr, 1997), and neuronal cell death associated with Alzheimer's disease (Berridge, 2014; Bezprozvanny & Mattson, 2008; Khachaturian, 1989; LaFerla, 2002; Gutierrez-Merino *et al.*, 2014; Liang & Wei, 2015). The $[Ca^{2+}]_i$ is mainly determined by the calcium influx through membrane voltage-gated calcium channels and ryanodine channel-mediated calcium release from intracellular calcium stores (Gutierrez-Merino *et al.*, 2014). Dantrolene, a specific inhibitor of ryanodine channel-mediated calcium release from intracellular stores, directly and indirectly affects the level of $[Ca^{2+}]_i$. The changes in $[Ca^{2+}]_i$ indirectly affect the ionic currents such as L-type calcium current (Imredy & Yue, 1994), calcium-activated potassium currents (Vergara *et al.*, 1998; Adams *et al.*, 1982), and the hyperpolarization-activated current (h-current) (Hagiwara & Irisawa, 1989; Destexhe *et al.*, 1993; Luthi & McCormick, 1998 ; Berridge, 2014). These changes of ionic currents can affect

the spike shape, which determines how much calcium enters into the cell (Gillette *et al.,* 1980; Augustine, 1990; Estes *et al.,* 2014). In this study we analyzed the changes of the spike width and minimum after-hyperpolarization potential (mAHP) caused by indirect effects of dantrolene. We investigated the cellular mechanism controlling the spike width and calcium influx through voltage-gated calcium channels and their effects on $[Ca^{2+}]_i$.

By applying dantrolene, we assess the role of intracellular calcium stores in the dynamics of spike generation. The application of dantrolene first gradually changed the spike shapes and eventually silenced the B5 neurons of the mollusk *Helisoma trivolvis* (Artinian *et al.*, unpublished data). During this process, the spike width gradually decreased and the mAHP was shifted towards more hyperpolarized voltages. Also, the dantrolene treatment had an inhibitory effect on two inward currents: the h-current and persistent sodium current. We attribute the inhibition of the h-current to the change in $[Ca^{2+}]_i$. The voltage of half-activation of the h-current is calcium-dependent (Hagiwara & Irisawa, 1989; Destexhe *et al.,* 1993; Luthi & McCormick, 1998; Berridge, 2014). Therefore, the decrease in $[Ca^{2+}]_i$ shifts the activation curve of the h-current towards more negative values and indirectly reduces the amount of the h-current (Hagiwara & Irisawa, 1989; Destexhe *et al.,* 1993; Luthi & McCormick, 1998; Berridge, 2014). We investigated the questions how changes in these two inward currents affect the spike shape, what cellular mechanisms govern the changes in the spike shape, and whether these changes affect the $[Ca^{2+}]_i$.

We developed a biophysical Hodgkin-Huxley-type model of B5 neurons and investigated how the manipulations of the h-current and persistent sodium current would affect the spike shape. Since dantrolene lowers the $[Ca^{2+}]_i$, we modeled the dantrolene effects on the h-current by shifting its voltage of half-activation towards more negative values. We showed that the

inhibition of the h-current reduces the spike width and shifts mAHP towards more hyperpolarized voltages. We also demonstrated similar changes in the spike shape as persistent sodium current was removed from neuronal activity. The observed alterations of the spike shape, caused by either removal of the h-current or down-regulation of the persistent sodium current, closely matched the changes in spike shape observed after dantrolene treatment. Our model study suggests that treatment with dantrolene, resulting in a reduction of calcium release from intracellular stores, could indirectly affect the spike shape through inhibition of the h-current or persistent sodium current.

4.2 The mechanisms controlling the spike width

According to Hodgkin and Huxley (1952), the basic spike is generated by the interaction of fast sodium and potassium currents. In this mechanism the outward potassium currents control the repolarization part of the spike and determine the spike width. It is generally accepted that the contribution of the potassium currents is critical for the generation of functional narrow spikes. Although numerous studies describe that the blockade of outward currents contributes in spike broadening (Gillette *et al.*, 1982; Jackson *et al.*, 1991; Ma & Koester, 1995), we did not find any regulatory effects of outward current kinetics on the changes of spike width. It has been shown in many neurons, including R20 cells of *Aplysia californica* (Ma & Koester, 1995), Paracerebral neurons of *Pleurobranchaea* (Gillette *et al.*, 1982), and pituitary nerve terminals in rats (Jackson *et al.*, 1991), that the increase of spike width during high-frequency spiking can be explained by cumulative inactivation of potassium currents.

The comparison between the spike shapes of B5 and B19 neurons in buccal ganglia of *Helisoma trivolvis* shows that B5 neurons have much larger spike width compared to B19 neurons (Estes *et al.*, 2014). In B19 neurons the blockade of the potassium currents with

tetraethylamonium (TEA) and 4-aminopyridine (4AP) approximately doubled their spike width. The spikes were still much narrower compared to the spike width of B5 neurons in control condition. It is reported that spikes dominated by calcium currents are usually wider than the spikes dominated by sodium currents (Kim & Connors, 1993; Mackie & Meech, 1985). The spikes of B19 neurons are dominated by sodium current, while the spikes of B5 neurons are driven by calcium current (Artinian *et al.,* 2010). Therefore, the configuration of ionic currents can determine the spike shape and the spike width (Estes *et al.,* 2014).

The reduction in the level of $[Ca^{2+}]_i$ during dantrolene treatment decreases the amount of the calcium-dependent potassium currents. The decrease of these currents would cause an increase in spike width (Storm, 1987; Shao *et al.,* 1999). The opposite effect is recorded in dantrolene experiments; the spike width gradually decreases as the $[Ca^{2+}]_i$ is reduced in B5 neurons (Artinian *et al.,* unpublished data). Additionally, dantrolene did not affect the outward delayed rectifier current, which suggested that the changes in the spike width were controlled by inward currents. This consideration led us to the question whether the dynamics of inactivation of inward currents could explain the mechanism of the changes in the spike width.

In the B5 model, we investigated the mechanisms controlling the changes in the spike shape caused by the removal of the h-current, since dantrolene inhibited the h-current. The removal of the h-current decreases the spike frequency and narrows the spikes, whereas in other studies the narrower spikes correspond to higher frequencies (Carter & Bean, 2009). We found that the gating variables of outward currents did not noticeably affect the spike width, and only the variables of inward currents could explain the changes in the spike width. We demonstrated that at the spike threshold, the inactivation variables of three inward currents namely: fast sodium, persistent sodium, and calcium currents controlled the spike width. Carter and Bean

(2011) describe a similar mechanism in cerebellar Purkinje neurons, where the inactivation of inward sodium current governs the changes of the spike properties. They showed that the incomplete inactivation of sodium current resulted in larger frequencies of spiking activity (Carter and Bean, 2011). Similarly, we found that the spiking activity with higher frequency was associated with larger values of inactivation variables of inward currents. They report that broader spike width produces more complete inactivation of sodium current. In contrast, in our model the smaller values of inactivation variables of inward currents at the threshold caused narrower spike width.

It also has been shown that calcium currents have a direct effect on the value of the spike width (Storm, 1987; Alderich, 1981). Storm (1987) suggests that the spike width of rat hippocampal pyramidal neurons depends on calcium-activated potassium currents. The noticeably increased spike width, due to blockade of calcium-activated potassium current (TEA), is reduced by applying calcium-channel blockers (Storm, 1987). Even without applying TEA, the width of spike at the upper part of the action potential becomes narrower after the application of the calcium-channel blocker (Storm, 1987). One of the differences between our findings and the previously described mechanisms is that the values of the inactivation variables of the three inward currents are regulated by the activation of the h-current, which in result modulates the spike width.

4.3 The spike width determines the calcium influx

In the model, we report a linear correlation between calcium influx and the spike width; the increase in the spike width causes a large increase in calcium influx. Similarly, Augustine (1990) has shown that the presynaptic spike broadening causes a large increase in presynaptic calcium current; one percent increase in presynaptic spike width causes a seven percent increase

in presynaptic calcium current. The spike broadening enhances the postsynaptic current, which indicates that the spike broadening indirectly plays an important role in neurotransmitter release (Augustine, 1990). The changes in presynaptic spike width have a large regulatory effect on synaptic efficacy (Kandel & Schwartz, 1982; Hochner *et al.,* 1986), which is shown in numeral experiments including squid terminals (Katz & Miledi, 1967; Llinas *et al.,* 1981) and *Aplysia* nerve cell bodies (Hochnerl *et al.,* 1986).

In our model, the regulation of the h-current controlled the spike width and the changes in the spike width have a positive effect on calcium influx into the cell. It indicates that the h-current might have an important role in neurotransmitter release. The presynaptic hyperpolarization-activated channels have important roles in neurotransmitter release in hippocampal mossy fiber (Mellor *et al.,* 2002), in hippocampal interneurons (Lupica *et al.,* 2001), and synaptic plasticity (Beaumont & Zucker, 2000).

4.4 The role of calcium on homeostasic regulation of neuronal activity

The $[Ca^{2+}]_i$ is an important factor in homeostasis of neuronal activity (Liu *et al.,* 1998; Marder & Prinz, 2002; Gunay & Prinz, 2010). The spiking activity could be monitored by intracellular calcium sensors operating on different time scales (Liu *et al.,* 1998; Marder & Prinz, 2002; Gunay & Prinz, 2010). The $[Ca^{2+}]_i$ could govern the conductances of the membrane ionic currents to maintain functional patterns of electrical activity (Liu *et al.,* 1998; Marder & Prinz, 2002; Gunay & Prinz, 2010). This maintained activity is regulated through intracellular sensors detecting the changes in neuronal activity on the scales of bursting period (Marder & Prinz, 2002; Gunay & Prinz, 2010). The $[Ca^{2+}]_i$ is one of the main factors in activity-dependent homeostatic regulation because the calcium influx into the cell strongly correlates with electrical activity (Ross, 1989; Liu *et al.,* 1998). For example, if a neuron produces a too low level of

activity, the regulatory feedback of membrane currents will upregulate the depolarizing currents and down-regulate the hyperpolarizing currents in response to the low level of intracellular calcium concentration (Marder & Prinz, 2002). The up- and down-regulation of depolarizing and hyperpolarizing currents are opposite, if the activity level of a neuron is too high (Marder & Prinz; 2002).

4.5 Implication of the described mechanism in treatment of certain diseases

Calcium dynamics have been implicated in diseases such as Alzheimer's disease (Berridge, 2014; Bezprozvanny & Mattson, 2008; Khachaturian, 1989; LaFerla, 2002) and epilepsy (Raza *et al.*, 2004). The deregulation of calcium signaling, which results to an increase in cytosolic calcium concentration, is known in the case of Alzheimer's disease (Berridge, 2014; Bezprozvanny & Mattson, 2008; Khachaturian, 1989; LaFerla, 2002). Growing evidence suggests that dantrolene, which reduces the $[Ca^{2+}]_i$, has therapeutic effects in Alzheimer's disease (Peng *et al.*, 2012; Berridge, 2014; Liang & Wei, 2015). With our study, we emphasize that drugs targeting calcium stores might have direct and indirect effects in Alzheimer's disease. Direct effects target calcium channel pumps and calcium leak channels and indirect treatments could have significant influence on this disease through the regulation of ionic channels on the cell membrane.

We showed that blockade of the h-current reproduced the effects of dantrolene on spike shape and reduced the calcium influx into the cell. The calcium influx through voltage-gated calcium channels amplifies the activation of ryanodine receptors of endoplasmic reticulum stores and increases the calcium release into the cell (Popugaeva & Bezprozvanny, 2013; Goussakov *et al.*, 2011). Thus, we suggest that blockade of the h-current, which causes a decline in calcium influx, might reduce the activity of calcium-induced calcium release from intracellular stores. In

particular, we predict that the regulation of the h-current could have positive therapeutic effects in Alzheimer's disease. We believe that the computer modeling will help us to understand the precise neuronal dynamics and be able to apply the dynamics in designing effective treatments targeting Alzheimer's disease.

5 CONCLUSIONS

We developed a model of B5 neurons, which reproduced the electrical activity of these neurons under different pharmacological treatments. The removal of the h-current or down-regulation of the persistent sodium current decreased the spike width and shifted the mAHP to more hyperpolarized voltages, reproducing the effects of dantrolene on spike shape. We found in the model that the calcium influx linearly correlated with the spike width and decreased for narrower spikes. The inactivation variables of fast sodium, persistent sodium, and calcium currents at the threshold governed the spike width. The value of these variables were determined by the activation of the h-current.

REFERENCES

1. **Adams P.R., Constanti A., Brown D.A., and Clark R.B.,** Intracellular Ca^{2+} activates a fast voltage-sensitive K^{+}-current in vertebrate sympathetic neurons, *Nature (London), 296:746-749, 1982.*

2. **Albert B., Johnson A., Lewis J., Raff M., Roberts K and Walter P.,** Molecular Biology of the Cell, 4th edition, New York: Garland Science; 2002.

3. **Alderich R.W., Getting P.A., Thompson S.H.,** Mechanism of frequency-dependent broadening of molluscan neuron soma spikes, *J Physiol (London), 291:531-544, 1979.*

4. **Artinian L., Tornieri K., Zhong L., Baro D. and Rehder V.,** Nitric Oxide Acts as a Volume Transmitter to Modulate Electrical Properties of Spontaneous Firing Neurons via Apamin-Sensitive Potassium Channels, *Journal of Neuroscience, 4511-09, 2010.*

5. **Artinian L., Zhong L., Yang H., and Rehder V.,** Nitric oxide as intracellular modulator internal production of NO increases neuronal excitability via modulation of several ionic conductances, *European Journal of Neuroscience, doi: 10.1111/j.1460-958, 2012.*

6. **Artinian L., Ghabel H., Zhong L., Estes S., Cymbalyuk G.,** and **Rehder V.,** The tonic intracellular calcium release from ryanodine channels define regenerative neuronal spiking via up-regulation of hyperpolarization-activated current and persistent sodium current, *unpublished data.*

7. **Augustine G.T.,** Regulation of transmitter release at the squid giant synapse by presynaptic delayed rectifier potassium current, *J Physiol (London), 431:343-364,1990.*

8. **Baker K.D., Edwards T.M. and Rickard N.,** The role of intracellular calcium stores in synaptic plasticity and memory consolidation, *J Neurbiorev, doi:10.1016, 2013.*

9. **Barnett W.H., O'Brien G., and Cymbalyuk G.,** Bistability of silence and seizure-like bursting, *J Neuroscience Methods, 220(2):179-89, doi: 10.1016/j.jneumeth, 2013*

10. **Barnett W.H. and Cymbalyuk G.,** A codimension-2 Bifurcation Controlling Endogeneous Bursting Activity and Pulse-Triggered Responses of a Neuron Model, *PLosONE, doi:10.1371, 2014.*

11. **Baxter D.A., Canavier C.C., Clark J.W. and Byrne J.H.,** Computational Model of Serotonergic Modulation of Sensory Neurons in Aplysia, *Journal of Neurophysiol. 82:2914-2935, 1999.*

12. **Beaumont A.** and **Zucker R.S.,** Enhancement of synaptic transmission by cyclic AMP modulation of presynaptic I_h channels, *Nature Neuroscience, 3, 133-141, 2000.*

13. **Berridge M.J., Bootman M.D. and Roderick L.,** Calcium Signaling Dynamics, Homeostasis and Remodelling, *Nature Reviews Molecular Cell Biology*, volume 4, 2003.

14. **Berridge M.J.,** Neural Calcium Signaling, *Neuron, vol. 21, pp. 13-26, 1998.*

15. **Berridge M.J.,** Calcium hypothesis of Alzheimer's disease, *European Journal of Physiology, vol. 459, Issue 3, pp. 441-449, 2010.*

16. **Berridge M.J.,** Calcium regulation of neural rhythms, memory and Alzheimer's disease, *J. Physio, 592.2, pp 281-293, 2014.*

17. **Bezprozvanny I.** and **Mattson M.P.,** neural calcium mishandling and the pathogenesis of Alzheimer's disease, *Trends Neurosci 31:454-463, 2008.*

18. **Bungay Sh.D. and Campbell S.A.,** Modelling a respiratory central pattern generator neuron in Lymnaea Stagnalis, *Canadian Applied Mathematics Quaterly, volume 17, number 2, 2009.*

19. **Butera R.J., Clarck J.W., Canavier C.C., Baxter D.A. and Byrne J.H.,** Analysis of the effects of modulatory agents on a modeled bursting neuron: Dynamic interactions between voltage and calcium dependent system, *J Comput Neurosci, vol.2, NO. 1, pp. 1-44, 1995.*

20. **Carter B.C.** and **Bean B.P.,** Sodium entry during action potential of mammalian central neurons: incomplete inactivation and reduced metabolic efficiency in fast-spiking neurons, *J Neuron, 64, 898-909, 2009.*

21. **Carter B.C.** and **Bean B.P.,** Incomplete inactivation and rapid recovery of voltage-dependent sodium channels during high-frequency firing in Cerebellar Purkinje neurons, *J Neurophysiol, 105:860-871, 2011.*

22. **Cymbalyuk G., Gaudry Q., Masino M.A.,** and **Calabrese R.L.,** Bursting in leech heart interneurons: cell-autonomous and network-based mechanisms, *J Neurosci, 22(24): 10508-92, 2002.*

23. **Destexhe A., Babloyantz A. and Sejnowski T.J.,** Ionic mechanisms for intrinsic slow oscillations in thalamic relay neurons, *Biophys J., vol. 65(4), pp. 1538-1552, 1993.*

24. **DiFreancesco D.,** The role of the funny current in pacemaker activity, *Circulation Research, vol. 106, pp. 434-446, 2010.*

25. **DiFrancesco D., Ferroni A., Mazzanti M., and Tromba C.,** Properties of the hyperpolarizing-activated current (if) in cells isolated from the rabbit sino-atrial node, *J Physiol., 377:61-88, 1986.*

26. **Estes S., Zhong L.R., Artinian L. and Rehder V.,** The Role of Action Potentials in Determining Neuron-Type-Specific Responses to Nitric Oxide, *Developmanetal Neurobiology, doi: 10.1002/dneu.22233, 2014.*

27. **Gillette R., Gillette M.U., Davis W.J.,** Substrates of command ability in a buccal neuron of *Pleurobranchaea.* I. Mechanisms of action potential broadening, *J Neurophysiol, 47:885-908, 1980.*

28. **Gillette R., Kovac M.P., Davis W.J.,** Control of feeding motor output by Paracerebral neurons in brains of *Pleurobranchaea californica. J Neurophysiol, 47:885-908, 1982*.

29. **Goussakov I., Miller M.B., and Stutzmann G.E.,** NMDA-mediated Ca^{2+} influx drives aberrant ryanodine receptor activation in dendrites of young Alzheimer's disease mice, *J Neurosci, 30(36): 12128-12137, 2011*.

30. **Gunay C.** and **Prinz A.A.,** Model calcium sensors for network homeostasis: sensors and readout parameter analysis from a database of model neuronal networks, *J Neurosci, 30(5): 4686-4698, 2010.*

31. **Gutierrez-Merino C., Marques-da-Silva D., Fortaleza S, and Samhan-Arias A.,** Cytosolic Calcium Homeostasis in Neurons - Control systems, Modulation by Reactive Oxygen and Nitrogen Species, and Space and Time Fluctuations, Neurochemistry, doi:10.5772/57576, ISBN: 978-953-51-1237-2, 2014.

32. **Guttman R., Lewis S.** and **Rinzel J.,** Control of repetitive firing in squid axon membrane as a model for a neurons oscillator, *J Physiol, vol. 305, pp. 377-395, 1980.*

33. **Hagiwara N.** and **Irisawa H.,** Modulation by Intracellular Calcium of the Hyperpolarization-Activated inward Current in Rabbit Single Sino-Atrial Node Cells, *Journal of Physiology, 409 , pp. 121-141, 1989.*

34. **Hasenstaub A., Otte S., Callaway E.,** and **Sejnowski T.J.,** Metabolic cost as a unifying principle governing neuronal biophysics, *PNAS, vol. 107, No. 27, 12329-12334,2010.*

35. **Hill A., Le J, Masino M, Olsen O,** and **Calabrese R,** A model of a segmental oscillator in leech heartbeat neuronal network. *J Comput Neurosci 10:281-302, 2001*.

36. **Hille B.**, Ionic channels of excitable membranes, 2nd edition, *1991*.

37. **Hochner B., Klein M., Schacher S.,** and **Kandel E.R.,** Action potential duration and the modulation of transmitter release from the sensory neurons of*Aplysia* in presynaptic facilitation and behavioral sensitization, *Proceedings of the National Academy of Science of the USA, 83, 8410-8414, 1986.*

38. **Hodgkin A.L.** and **Huxley A.F.,** A quantitative description of membrane current and its application to conduction and excitation in nerve, *J Physiol, 117, 500-544,1952.*

39. **Imredy J.P.** and **Yue D.T.,** Mechanism of Ca^{2+} - sensitive inactivation of L-type Ca^{2+} channels, *Neuron, vol. 12, issue 6, pp. 1301-131, 1994.*

40. **Inan S.** and **Wei H.,** The Cytoprotective Effects of Dantrolene: A Ryanodine Receptor Antagonist, *volume 111, Issue 6, pp. 1400-1410, 2010.*

41. **Jackson M.B., Konnerth A., Augustine G.J.,** Action potential broasdening and frequency-dependent fadilitation of calcium signals in pituitary nerve terminals *Proc Natl Acad Sci USA 88:380:384, 1991.*

42. **Kandel E.R.** and **Schwartz J.H.,** Molecular biology of learning: modulation of transmitter release, *Science, 229, 433-443, 1982.*

43. **Katz B.** and **Miledi R.,** A study of synaptic transmission in the absence of nerve impulses. *J Physiol, 192, 407-436, 1967.*

44. **Khachaturian Z.S.,** Calcium, membrane, aging, and Alzheimer's disease, Introduction and overview, *Ann N Y Acd Sci,568,1-4, 1989.*

45. **Kim H.G.** and **B.W. Connors,** Apical Dentrites of the Neocortex: correlation between Na- and Ca-dependent spiking and pyramidal cell morphology, *J Neurisci, 13(12): 5301-5311, 1993.*

46. **LaFerla F.M.,** Calcium dyshomeostasis and intracellular signaling in Alzheimer's disease, *Nat Rev Neurosci, 3,862-872, 2002.*

47. **Liang L.** and **Wei H.,** Dantrolene, a treatment for Alzheimer disease?, *Alzheimer Dis Assoc Disord.,29(1); 1-5, 2015.*

48. **Liu Z., Golowasch J., Marder E.,** and **Abbott L.F.,** A Model Neuron with Activity-Dependent Conductancees Regulated by Multiple Calcium Sensors, *J Neurosci, 18(7):2309-2320, 1998.*

49. **Llinas R., Steinberg I.Z.,** and **Walton K.,** Relationship between presynaptic calcium current and post-synaptic potential in squid giant synapse. *Biophysical Journal, 16, 83-86, 1981.*

50. **Lopez J.R., Lyckman A., Oddo S., LaFerla F.M., Querfurth H.W., Shtifman A.,** Increased interneuronal resting [Ca^{2+}] in adult Alzheimer's disease mice, *Journal of Neurochemistry, 105, pp. 262-271, 2008.*

51. **Lupica C.R., Bell J.A., Hoffman A.F.,** and **Watson P.L.,** Contribution of hyperpolarization-activated current (I_h) to membrane potential and GABA release in Hippocampal interneurons, *J Neurophysiol, vol. 86, No.1, 261-268, 2001.*

52. **Luthi A.,** and **McCormick D.A.,** Ca^{2+}-mediated up-regulation of I_h in the Thalamus, *Annals of the New York Academy of Sciences, vol 868, Molecular and Functional diversity of ion channels and receptors, pp. 765-769,1998.*

53. **Ma M.** and **Koester J.,** Consequences and Mechanisms of Spike Broadening of R20 Cells in *Aplysia californica, Journal of Neuroscience, 15(10): 6720-6734, 1995.*

54. **Ma M.** and **Koester J.,** The Role of K+ Crrents in Frequency-Dependent Spike Broadening in *Aplysia* R20 Neurons: A Dynamic-Clamp Analysis, *Journal of Neuroscience, 16(13): 4089-4101, 1996.*

55. **Mackie G.O.** and **Meech R.W.,** Separate sodium and calcium spikes in the same axon, *Nature, 313, 791-793, 1985.*

56. **Malaschenko T., Shilnikov A.,** and **Cymbalyuk G.,** Bistability of bursting and silence regimes in a model of a leech heart interneuron, *Phys Rev, E 84, 041910, 2011.*

57. **Marder E.** and **Prinz A.A.,** Modeling stability in neuron and network function: the role of activity in homeostasis, *BioEssays, 24:1145-1154, 2002.*

58. **Mellor J., Roger A.N.,** and **Schmitz D.,** Mediation of Hippocampal Mossy Fiber Long-Term Potantiation by Presynaptic I_h Channels, *Science, vol. 295, No. 5552, 143-137, doi: 10.1126/science.1064285, 2002.*

59. **Peng J., Liang G., Inan S., Wu Z., Joseph D.J., Meng Q., Peng Y., Eckenhoff M.F.,** and **Wi H.,** Dantrolene ameliorates cognitive decline and neuropathology in Alzheimer triple transgenic mice, *Neuroscience Letters, doi:10.1016, 2012.*

60. **Popugaeva E.** and **Bezprozvanny I.,** Role of endoplasmic reticulum Ca^{2+} signaling in the pathogenesis of Alzheimer disease, *Front Mol Neurosci, v.6, PMC3776136,doi: 10.3389/fnmol.2013.00029, 2013.*

61. **Raza M., Blair R.E., Sombati S., Carter D.S., Deshpande L.S.,** and **DeLorenzo R.J.,** Evidence that injury-induced changes in hippocampal neuronal calcium dynamics during epileptogenesis cause acquired epilepsy, *PNAS, vol. 101, Np. 50, 17522-17527, 2004.*

62. **Rehder V.** and **Kater S.B.,** Regulation of neuronal growth cone filopodia by intracellular calcium, *Journal of Neuroscience, 12, pp. 3175-3186, 1992.*

63. **Ross W.M.,** Changes in intracellular calcium during neuron activity, *Annu Rev Physiol, 51:491-506, 1989.*

64. **Sabati B.L.** and **Regehr W.G.,** Control of neurotransmitter release by presynaptic waveform at Granule cell to Purkinje cell synapse, *J Neurosci, 17(10): 3425-3435, 1997.*

65. **Sekerli M, Del Negro C.A., Lee R.H.,** and **Butera R.,** Estimating action potential thresholds from neuronal time-series: New metrics and evaluation of methodologies, *IEE Transaction on Biomedical Engineering, vol. 51, NO. 9, 2004.*

66. **Shao L., Halvorsrud R., Borg-Graham L.,** and **Storm J.F.,** The role of BK-type Ca2+-dependent K+ channels in spike broadening during repetitive firing in rat hippocampal pyramidal cells, *J Physiol, vol. 521, Issue 1, pp. 135-146, 1999.*

67. **Shilnikov A. and Cymbalyuk G.,** Transition between tonic spiking and bursting in a neuron model via blue-sky-catastrophe, *Physic Review Letters 94, 048101, 2005.*

68. **Shilnikov A., Calabrese R. and Cymbalyuk G.,** Mechanisms of bistability: Tonic spiking and bursting in a neuron model, *Physic Review E 71, doi:10.1103, 2005.*

69. **Storm J.F.,** Action potential repolarization and a fast after-hyperpolarization in rat hippocampal pyramidal cells, *J Physiol., 385, pp. 733-759, 1987.*

70. **Vergara C., Latorre R., Marrion N.V.,** and **Adelman J.P.,** Calcium-activated potassium channels, *Current Opinion in Neurobiology, vol. 8, Issue 3, pp. 321-329, 1998.*

71. **Zhong L., Artinian L., Rehder V.,** Dopamine suppresses neuronal activity of Helisoma B5 neurons via a D2-like receptor, activity PLC and K channels, *J Neurosci, 2013.*

72. **Zhong L., Estes S., Artinian L., Rehder V.,** Nitric Oxide Regulates Neuronal Activity via Calcium-Activated Potassium Channels, *Journal PLosONE 8(11), 2013.*

73. **Zheng J.Q. and Poo M.,** Calcium Signaling in Neuronal Motility, *Annual Review of Cell and Developmental Biology, vol. 23; 375-404, 2007.*

APPENDIX

The Hodgkin-Huxley-type model of *Helisoma trivolvis* B5 neurons is developed describing the dynamics of ionic currents. The dynamics of membrane potential is described as follow:

$$C_m \frac{dV}{dt} = -I_{NaF} - I_{NaP} - I_K - I_{Ka} - I_{K4} - I_{SK} - I_{BK} - I_{Ca} - I_H - I_L + I_{inj} \qquad (1)$$

where C_m is the total membrane capacitance ($1\times10^{-9} F$) and I_{inj} is the injected current. These ionic currents are represented by:

$$I_{NaF} = G_{NaF} m_{\infty NaF}^3 h_{NaF} \left[V - E_{Na}\right] \qquad (2)$$

$$I_{NaP} = G_{NaP} m_{NaP}^3 h_{NaP} \left[V - E_{Na}\right] \qquad (3)$$

$$I_K = G_K m_K^4 \left[V - E_K\right] \qquad (4)$$

$$I_{Ka} = G_{Ka} m_{Ka}^2 h_{Ka} \left[V - E_K\right] \qquad (5)$$

$$I_{K4} = G_{K4} m_{K4}^4 \left[V - E_K\right] \qquad (6)$$

$$I_{SK} = G_{SK} \left[V - E_K\right] \qquad (7)$$

$$I_{BK} = G_{BK} m_{BK} \left[V - E_K\right] \qquad (8)$$

$$I_{Ca} = G_{Ca} m_{Ca} h_{Ca} \left[V - E_{Ca}\right] \qquad (9)$$

$$I_H = G_H m_H^2 \left[V - E_H\right] \qquad (10)$$

$$I_L = G_L \left[V - E_L\right] \qquad (11)$$

where G_{ion} is the maximal conductance, E_{ion} is the reversal potential, and m and h are activation and inactivation gating variables respectively. The gating variables are generated by the following equation:

$$\frac{dy_{ion}}{dt} = \frac{y_{\infty ion}(V) - y_{ion}}{\tau_{yion}(V)} \tag{12}$$

where $y_{\infty ion}$ is the steady-state activation or inactivation and τ_{yion} is the time constant for each of the ionic currents. The equation below describes the steady-state activation or inactivation curves in the model:

$$y_{\infty ion} = \frac{1}{1 + \exp\left(\frac{V - V_{1/2yion}}{k_{yion}}\right)} \tag{13}$$

Here, $V_{1/2yion}$ is the voltage, where the steady state activation or inactivation curve reach 0.5 and k_{yion} describes the steepness of the curve. The activation and inactivation time constants are voltage-independent except for activation time constants of I_K, I_{Ka} and I_{NaP}. These voltage-dependent time constants are described as below:

$$\tau_j(V) = \frac{\tau_{0j}\exp\left(\frac{\delta_j\left(V - V_{1/2yj}\right)}{k_{yj}}\right)}{1 + \exp\left(\frac{V - V_{1/2yj}}{k_{yj}}\right)} \tag{14}$$

$$\tau_{mNaP} = 0.0117 + 0.004 \times 10^{-3} \times \exp\left(-\frac{V}{7.6}\right) \tag{15}$$

where j is either K or Ka. The canonical parameter values are presented in Table A.1.

The equation to calculate the calcium influx ($[Ca]_i$) for time duration of 5 seconds spiking activity is shown below:

$$[Ca]_i = \frac{\sum_{n=1}^{N}[-I_{Ca}]_n \times dt}{2F \times vol} \quad (16)$$

where *F* and *vol* are the Faraday constant and volume of the B5 neuron, respectively. N corresponds to the number of points on spiking activity for 5 seconds and dt is the integration time step.

Table A.1 Parameter values for canonical model of B5 neurons.

ion	y_{ion}	G_{ion} (nS)	E_{ion} (mV)	$V_{1/2yion}$ (mV)	k_{yion} (mV)	τ_{0ion}	δ_{ion}	t_y (s)
NaF	$m_{\infty\text{-}NaF}$	220	130	-23.3	-7.5			
	h_{NaF}			-35	5			0.04
NaP	m_{NaP}	110	130	-35	-6.8			
	h_{NaP}			-58	4			0.1
K	m_K	117	-75	-28	-5.7	0.08	0.83	
Ka	m_{Ka}	40	-75	-34.5	-8.8	0.012	0.087	
	h_{Ka}			-66	8.5			0.15
K4	m_{K4}	180	-75	-20	-8			0.005
BK	m_{BK}	1	-75	-45	-10.5			0.001
SK		0.8	-75					
Ca	m_{Ca}	81	111	-21.7	-5			0.0035
	h_{Ca}			-41	3			0.09
H	m_H	10	-21	-54.5	10.5			1
L		8	-51					

Table A.2 Parameters of calcium influx.

dt (s)	vol (L)	F (sA/mol)
0.0001	7.9×10^{-9}	96485.3